IJCRT.ORG ISSN : 2320-2882

INTERNATIONAL JOURNAL OF CREATIVE RESEARCH THOUGHTS (IJCRT)

An International Open Access, Peer-reviewed, Refereed Journal

MIXED CONVECTIVE PRANDTL NANOFLUID FLOW OVER A STRETCHING SHEET IN THE PRESENCE OF THERMAL AND SOLUTAL BIOT NUMBERS: OPTIMAL SOLUTION

*[1]Srikantha Setty B, [2]Ramanjini V

[1]Assistant Professor, Department of Mathematics, Navodaya Institute of Technology, Raichur, India
[2]Former research Scholar, Department of Studies in Mathematics, VSKU Ballari, India.

Abstract: The present article is to investigate the effects of two dimensional magneto hydrodynamic mixed convective Prandtl nanofluid flow, heat and mass transfer over a stretching sheet in the presence of convection; heat generation/absorption, chemical reaction and velocity slip boundary condition. The governing nonlinear partial differential equations are reduced into set of ordinary differential equation through appropriate similarity transformation. Further, solutions are obtained via Optimal Homotopy Analysis method. The obtained results are presented graphically in order to analyze the features of the involved key parameters which are controlling the flow model. The skin friction coefficient, Nusselt number and Sherwood number are also discussed in detail. Further, validation of the present work is verified with earlier published articles and found to be in excellent manner. It is noticed that Prandtl fluid parameter increases the velocity of the fluid whereas slightly decrement in fluid temperature. A temperature profile gets augmented in the case of Brownian and thermophoresis parameter.

Index Terms **- Prandtl nanofluid, stretching sheet, mixed convection, chemical reaction, OHAM.**

I. INTRODUCTION

The dynamics of liquid flow due to a stretching sheet is more application in industrial and technological domain namely paper production, plastic sheets, metal spinning, artificial fibers, glass cutting and many others. In view of these practical applications, Sakiadas (1961) initiated the study of boundary layer flow over a continuous stretching surface. Crane (1970) extended the work of Sakiadas (1961) by introducing the stretching sheet problem whose velocity is proportional to the distance from the slit. Based on his work many researchers further extended by considering different situations. Chen and Char (1988) studied effects of suction/blowing parameter over a continuous stretching sheet. Cortell (2005) examined the flow and heat transfer characteristics over a porous stretching surface in the presence of internal heat generation and absorption parameter. Abel and Mahesh (2008) studied magneto viscoelastic fluid due to a stretching sheet in the presence of variable thermal conductivity. Ishak et al. (2009) scrutinized unsteady flow and heat transfer due to a vertical stretching sheet. Prasad et al. (2012) investigated behavior of power law non-Newtonian fluid over a non linear stretching sheet. Effect of magneto tangent hyperbolic fluid and Eyring Powel fluid over a stretching surface has studied by Akbar et al. (2013)-(2015). Malik et al. (2015) examined MHD flow of tangent hyperbolic fluid over a stretching cylinder by using Keller box method. Rashidi et al.(2017) investigated magneto convective third grade flow over a stretching sheet with entropy. Recently, Khan et al. (2019) analyzed MHD heat generation Prandtl fluid flow due to a stretching surface and solutions are obtained from shooting method.

Nowadays research community facing the main task on development of efficiency of heat transfer analysis in some fluids. To lead this situation adding small quantity of solid particles to the fluids as a result thermophysical properties gradually improves. Because of this reason, researchers introduce the new concept known as nanofluids, these are nanoparticle suspensions made up of metals, oxides, carbides/carbon nanotubes etc. Choi (1995) was one of the first researcher who worked on the nanofluids. Buongiorno (2006) analyzed the flow and convective heat transfer phenomena of nanofluids and reveals that Brownian and thermophoresis parameter are the main parameters to enhance the heat transfer. Based on Boungiorno's model, many researchers worked by considering different physical geometries with various boundary conditions. Rana and Bhargava (2012) investigated numerical solution of nanofluid flow and heat transfer over a stretching sheet. Prasad et al. (2018) examined Williamson nanofluid flow over a slender elastic sheet using Cattanoe- Christov heat flux model. Uddin et al. (2018) studied the convective flow and heat transfer of nanofluid due to a stretching/shrinking sheet in presence of slip effects. Hayat et al. (2018) scrutinized effect of Darcy nanofluid flow over a non-linear stretching sheet and solutions are obtained via Homotopy Analysis Method. Recently, upper convected Maxwell nanofluid flow through a permeable channel using Boungiorno's model was analyzed by Prasad et al. (2020).

The problems of a mixed convection gained much attention due to its various applications in science and industrial sectors namely, electronic devices cooled by fans, solar receivers exposed to wind currents, cooling of nuclear reactors during emergency situation, drying technologies and many others. Moutsoglou and Chen (1980) examined the effects of buoyancy forces on continuous moving surface. Effect of mixed convective heat transfer over a stretching sheet in presence of suction/blowing was investigated by Vajravelu (1994). Das et al. (2015) studied the effect of magneto buoyancy forces over a porous plate with viscous dissipation. Recently, Prasad et al. (2019) analyzed the magneto mixed convection of Casson nanofluid over a slender rotating disk in presence of suction/injection.

It has been noticed that all the aforementioned investigators restricted their study on linear/ nonlinear stretching sheet with Prandtl nanofluid in the presence of thermal and solutal Biot numbers. Keeping these studies in mind, the aim of the present article is to analyze the study of Prandtl nanofluid flow, heat and mass transfer over a mixed convective linear stretching sheet in the presence of viscous dissipation and chemical reaction.The involved governing partial differential equations are converted into a set of ordinary differential equations with the help of appropriate similarity transformations. In this work we considered an optimal homotopy analysis method (OHAM) (see, Liao (2010), Fan and You (2013), Van Gorder (2019)) has been used for solving the solutions of coupled nonlinear differential equations. The physical behaviour of all the emerging parameters that arise in the governing flow problems are presented through graphs and tables. The obtained results are compared with the earlier published results and are found to be in excellent agreement.

II. MATHEMATICAL FORMULATION OF THE PROBLEMS

Consider the steady, two-dimensional, thermally stratified, incompressible flow of a viscous Prandtl nanofluid over a stretching sheet in the presence of buoyancy forces and velocity slip condition. Here the velocity of the stretching surface is assumed to be $U_w = cx$ where c is small physical parameter related to stretching sheet and the flow is subjected to a transverse magnetic field of strength B_0. Heat and mass transfer characteristics are analyzed by considering the effects of Brownian motion and thermophoresis phenomena along with thermal Biot number Bi_T and solutal Biot number Bi_C. The temperature and nanoparticle concentration at the surface of the Riga plate is defined as T_w and C_w respectively and further the ambient temperature and nanoparticle concentration are denoted as T_∞ and C_∞. Under these assumptions the boundary layer equations for continuity, momentum, energy and nanoparticle concentration are:

$$\frac{\partial u}{\partial x}+\frac{\partial \mathrm{v}}{\partial y}=0 \tag{1}$$

$$u\frac{\partial u}{\partial x}+\mathrm{v}\frac{\partial u}{\partial y}=\nu\frac{A}{C_1}\frac{\partial^2 u}{\partial y^2}+\frac{\nu A}{2C_1^3}\frac{\partial^2 u}{\partial y^2}\left(\frac{\partial u}{\partial y}\right)^2-\frac{\sigma B^2}{\rho}u+g\beta_T\left(T-T_\infty\right)+g\beta_C\left(C-C_\infty\right) \tag{2}$$

$$u\frac{\partial T}{\partial x}+\mathrm{v}\frac{\partial T}{\partial y}=\alpha_1\frac{\partial^2 T}{\partial y^2}+\tau\left[D_B\frac{\partial C}{\partial y}\frac{\partial T}{\partial y}+\frac{D_T}{T}\left(\frac{\partial T}{\partial y}\right)^2\right]+\frac{Q_0}{\rho c_p}\left(T-T_\infty\right)+\frac{\mu}{\rho c_p}\left(\frac{\partial u}{\partial y}\right)^2 \tag{3}$$

$$u\frac{\partial C}{\partial x}+\mathrm{v}\frac{\partial C}{\partial y}=D_B\frac{\partial^2 C}{\partial y^2}+\frac{D_T}{T_\infty}\frac{\partial^2 T}{\partial y^2}-K_1\left(C-C_\infty\right) \tag{4}$$

and the corresponding boundary conditions can be written as:

$$u=U+\alpha_2\frac{\partial u}{\partial y},,\ \mathrm{v}=0,\ -K\left(\frac{\partial T}{\partial y}\right)=h_T\left(T_w-T\right),-D_B\left(\frac{\partial C}{\partial y}\right)=h_C\left(C_w-C\right),\ \text{at}\ y=0,$$
$$u\to 0,\ T\to T_\infty,\ C\to C_\infty\quad \text{as}\ y\to\infty \tag{5}$$

Here *u* and v are the velocity components along the Cartesian coordinates *x* and *y* respectively, ν is the kinematic viscosity parameter, A and C_1 are physical parameters in Prandtl fluid, σ is the electric conductivity, ρ is the fluid density, g is the gravitational parameter, β_T thermal expansion coefficient, β_C concentration expansion coefficient, T and C are temperature and nanoparticle concentration of the fluid respectively, α_1 is the thermal diffusivity, τ is the ratio between the effective heat capacity of the nanoparticle material and heat capacity of the fluid, D_B is the Brownian diffusion coefficient, D_T is the thermophoresis diffusion coefficient, Q_0 is heat generation/absorption coefficient, c_p is the specific heat at constant pressure, μ is dynamic viscosity, K_1 is the reaction rate, K is the thermal conductivity, α_2 is the velocity slip parameter, h_T is heat transfer coefficient, h_C mass transfer coefficient.

The system of governing partial differential equations is transformed into set of ordinary differential equations by introducing the following similarity transformations.

$$\eta=y\sqrt{\frac{c_0}{\nu}},\ \psi=\sqrt{c_0\nu}xf'(\eta),\theta(\eta)=\frac{T-T_\infty}{T_w-T_\infty},\ \ \phi(\eta)=\frac{C-C_\infty}{C_w-C_\infty}. \tag{6}$$

With the help of these transformations, the velocity components u and v along x and y directions in the form of dimensionless stream function is given by:

$$u=\partial\psi/\partial y=c_0xf'(\eta),\ \mathrm{v}=-\partial\psi/\partial y=-\sqrt{\nu c_0}\,f, \tag{7}$$

Using the above defined similarity transformations and stream function, then Eqns. (2) - (5) and required boundary conditions reduced as follow,

$$\alpha f'''+\beta f'''f''^2+ff''-f'^2-Mnf'+\lambda_T\left(\theta+\lambda_C\phi\right)=0 \tag{8}$$

$$\theta''+\mathrm{Pr}\left[f\theta'+Nb\phi'\theta'+Nt\theta'^2+Ecf''^2+\lambda\theta\right]=0 \tag{9}$$

$$\phi'' + \left(\frac{Nt}{Nb}\right)\theta'' + Lef\,\phi' - LeKc\phi = 0 \tag{10}$$

$$\left.\begin{aligned} &f(\eta) = 0,\ f'(\eta) = 1 + \alpha_2 f''(\eta), \\ &\theta'(\eta) = Bi_T\left(\theta(\eta) - 1\right),\ \phi'(\eta) = Bi_C\left(\phi(\eta) - 1\right) \end{aligned}\right\} \text{ at } \eta = 0, \tag{11}$$

$$f'(\eta) \to 0,\ \ \theta(\eta) \to 0,\ \ \phi(\eta) \to 0, \qquad \text{as } \eta \to \infty$$

The non-dimensional parameters $\alpha, \beta, Mn, \lambda_T, \lambda_C, \Pr, Nb, Nt, \lambda, Ec, Le, Kc, \alpha_2, Bi_T$ and Bi_C, appearing in the above equations are called, Prandtl fluid parameters, dimensionless parameter, thermal buoyancy parameter, concentration buoyancy parameter, Prandtl number, Brownian motion parameter, thermophoresis parameter, heat source/sink parameter, Eckert number, Lewis number, chemical reaction parameter, velocity slip parameter, thermal Biot number and solutal Biot number respectively. These parameters are mathematically expressed as,

$$\alpha = \frac{A}{C_1},\ \ \beta = \frac{Ac_0^2 x}{2C_1^2 \nu},\ \ Mn = \frac{\sigma B^2}{\rho c_0},\ \lambda_T = \frac{gB_T}{c_0},\ \lambda_C = \frac{B_C\left(C_w - C_\infty\right)}{B_T\left(T_w - T_\infty\right)},$$

$$\Pr = \frac{\nu}{\alpha_1},\ Nb = \frac{\tau D_B (C_w - C_\infty)}{\nu},\ Nt = \frac{\tau D_T (T_w - T_\infty)}{\nu T_\infty},\ \lambda = \frac{Q_0}{\rho c_0 c_p},\ Ec = \frac{c_0 x}{c_p\left(T_w - T_\infty\right)}, \tag{12}$$

$$Le = \frac{\nu}{D_B},\ Kc = \frac{K_1}{c_0}, \alpha_2 = \lambda_1\sqrt{\frac{c_0}{\nu}}\ \ Bi_T = \frac{h_T}{K}\sqrt{\frac{\nu}{c_0}} \text{ and } \ Bi_C = \frac{h_C}{D_B}\sqrt{\frac{\nu}{c_0}}$$

Physical quantities of interest: The important physical quantities of interest for the engineers such as drag force, heat transfer rate and mass transfer rate are calculated as follow.

$$C_{f_x} = \frac{\tau_w}{U_w^2},\ \ Nu_x = \frac{xq_w}{\alpha\left(T_w - T_\infty\right)},\ \ \ Sh_x = \frac{xj_w}{D_B\left(C_w - C_\infty\right)}$$

where $\tau_w = \nu\left[\frac{A}{C_1}\frac{\partial u}{\partial y} + \frac{A}{6C_1^3}\left(\frac{\partial u}{\partial y}\right)^3\right]$, $q_w = -\alpha\frac{\partial T}{\partial y}$ and $j_w = -D_B\frac{\partial C}{\partial y}$ at $y = 0$, respectively called wall friction, wall heat flux and wall mass flux. Using the governing similarity transformations, dimensionless form Skin friction coefficient, heat transfer coefficient and mass transfer coefficient reduces to the following form $\mathrm{Re}_x^{1/2} C_{f_x} = \left[\frac{\alpha\beta}{3} f'''(0) + \alpha f''(0)\right]$, $\mathrm{Re}_x^{-1/2} Nu_x = -\theta'(0)$ and $\mathrm{Re}_x^{-1/2} Sh_x = -\phi'(0)$, where $\mathrm{Re}_x = c_0 x/\nu$ is called local Reynolds number.

III. Semi-Analytical Method (OHAM)

In this study, the system of coupled nonlinear partial differential equations is converted into set coupled nonlinear ordinary differential equations. For solving these differential equations an efficient semi- analytical method called as an optimal homotopy analysis method (OHAM) (for details see, Liao (2010), Fan and You (2013), Van Gorder (2019)) is implemented. In order to get the solution of the system of these equations we choose the appropriate initial guesses and linear operators.

$$f_0(\eta) = (1/(1+\alpha_2))(1 - e^{-\eta}), \theta_0 = e^{-\eta},\ \phi_0 = e^{-\eta}, \tag{13}$$

$$L_f = \frac{d^3}{d\eta^3} - \frac{d}{d\eta}, L_\theta = \frac{d^2}{d\eta^2} - 1,\ L_\phi = \frac{d^2}{d\eta^2} - 1 \tag{14}$$

Optimal convergence control parameters: The non-zero auxiliary parameters known as convergence control parameters $\left(\hbar_f, \hbar_\theta, \hbar_\phi\right) \neq 0$, are necessary for convergence of solution series and these can be used to control the convergence region and the rate of convergence of the series solution. Therefore, optimal homotopy analysis method (OHAM) allows us an appropriate way to achieve the convergent solution. In order to get the optimized values of $\hbar_f$, $\hbar_\phi$ and $\hbar_\theta$, we introduce the concept of minimization by defining the averaged and total squared residual errors,

$$\left.\begin{aligned} E_n^f(\hbar_f) &= \frac{1}{M+1}\sum_{k=0}^{M}\left(\mathrm{N}_f\left[f_{[\mathrm{M}]}(\eta_k), \theta_{[\mathrm{M}]}(\eta_k), \phi_{[\mathrm{M}]}(\eta_k)\right]\right)^2 \\ E_n^f(\hbar_\theta) &= \frac{1}{M+1}\sum_{k=0}^{M}\left(\mathrm{N}_\theta\left[f_{[\mathrm{M}]}(\eta_k), \theta_{[\mathrm{M}]}(\eta_k), \phi_{[\mathrm{M}]}(\eta_k)\right]\right)^2 \\ E_n^f(\hbar_\phi) &= \frac{1}{M+1}\sum_{k=0}^{M}\left(\mathrm{N}_\phi\left[f_{[\mathrm{M}]}(\eta_k), \theta_{[\mathrm{M}]}(\eta_k), \phi_{[\mathrm{M}]}(\eta_k)\right]\right)^2 \end{aligned}\right\} \tag{15}$$

and $E_n^t = E_n^f + E_n^\theta + E_n^\phi$, $\delta y = 0.5,\ k = 20.$

The computational software such as Mathematica is used to minimizing these errors for $n = 1, 2, 3, \ldots$. Here we can clearly observe that the averaged and total squared residual errors reduces as order of the approximation increases, which confirms that OHAM exist successfully.

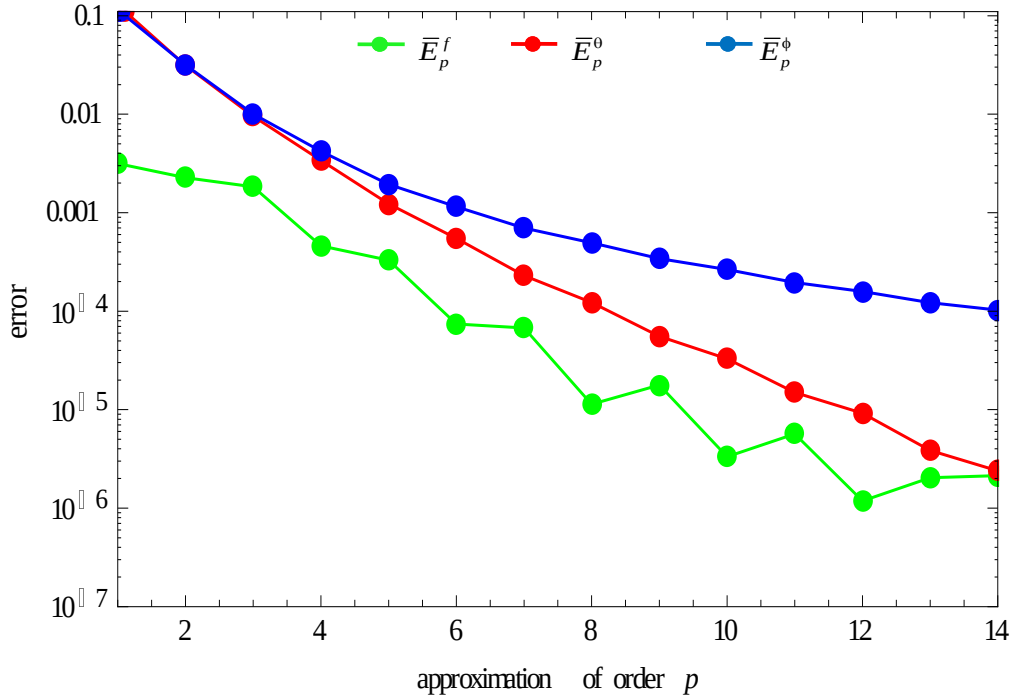

Fig.2a: Individual averaged squared residual errors versus order of approximation p.

Table1: Individual residual errors for the velocity, temperature and nanoparticle concentration distribution at a different order of approximation p.

p	$-\hbar_f$	$-\hbar_\theta$	$-\hbar_\phi$	E_p^t	CPU times **(S)**
1	0.0288	1.342	1.231	0.3524	0.557
4	1.8076	1.506	1.383	2.7×10^{-2}	9.114
8	1.9152	1.555	1.472	3.8×10^{-3}	70.88
10	1.9023	1.573	1.522	1.3×10^{-3}	139.43
14	1.7728	1.612	1.584	3.3×10^{-4}	384.65

Table.2: Optimal values of convergence control parameters and total squared residual errors for different approximation p.

p	$\overline{E}_p^f$	$\overline{E}_p^\theta$	$\overline{E}_p^\phi$	CPU time (s)
1	3.1×10^{-2}	12.8×10^{-2}	11.4×10^{-2}	0.557
4	4.6×10^{-4}	3.4×10^{-2}	4.21×10^{-2}	9.114
8	1.13×10^{-5}	1.22×10^{-3}	4.93×10^{-3}	70.88
10	3.32×10^{-6}	3.28×10^{-5}	2.62×10^{-4}	139.43
14	9.13×10^{-7}	2.39×10^{-6}	1.02×10^{-5}	384.65

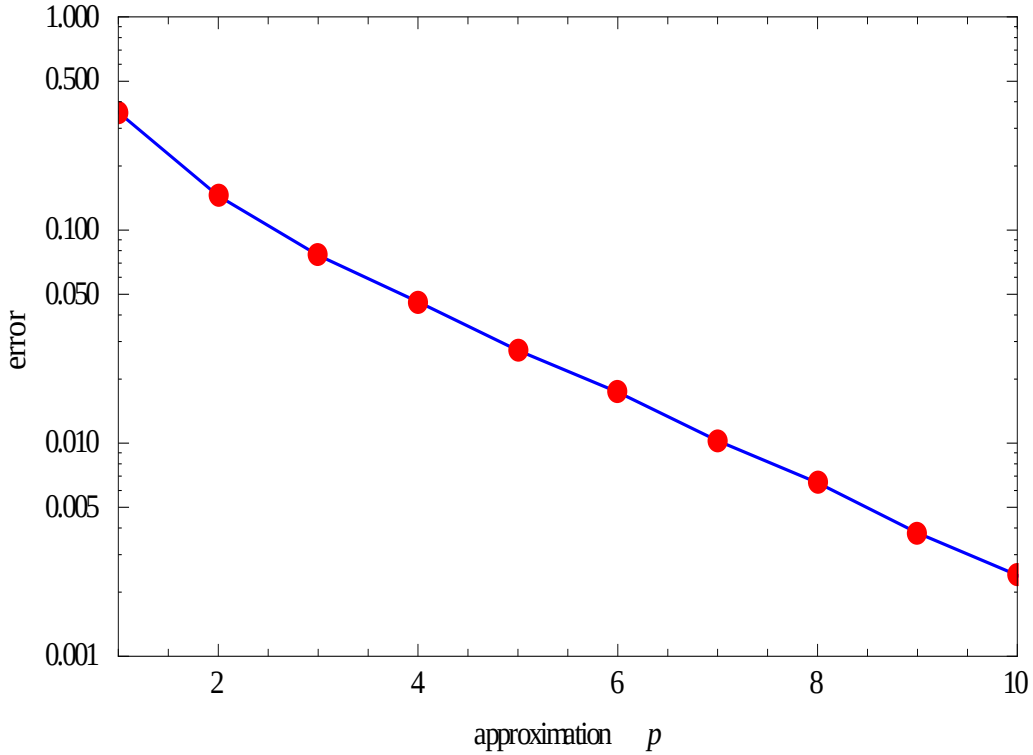

Fig.2b: Total averaged squared residual error versus order of approximation p

IV. Results and Discussion: The system of coupled non-linear partial differential equations (2) - (5) is converted into a set of ordinary differential equations (8) - (11) with the help of suitable similarity transformations (6) – (7) and then solved by semi-analytical method known as optimal homotopy analysis method. The influence of various physical parameters such as Prandtl fluid parameters α and β, Magnetic parameter Mn, thermal buoyancy parameter λ_T, concentration buoyancy parameter λ_C, Prandtl number $\Pr$, Brownian motion parameter Nb, thermophoresis parameter Nt, heat source/sink parameter λ, Eckert number Ec, Lewis number Le, chemical reaction parameter Kc, velocity slip parameter α_2, thermal Biot number Bi_T and solutal Biot number Bi_C on velocity profile $f'(\eta)$, temperature profile $\theta(\eta)$ and concentration profile $\phi(\eta)$ are exhibited through Figs.(2-9). Then the computed numerical values for the skin friction $f''(0)$, the Nusselt number $\theta'(0)$ and Sherwood number $\phi'(0)$ are also discussed in details and presented in Table 4.

Figs. 3(a-b) illustrate the effect of α and Mn, on $f'(\eta)$ and $\theta(\eta)$. It is noticed that $f'(\eta)$ enhances and $\theta(\eta)$ decreases for increasing values of α, whereas opposite characteristics are observed in the case of Mn. This is due to the fact that the drag forces called the Lorentz forces generated by the applied magnetic field which act as resistive drag forces opposite to the flow direction which results in a decrease in velocity. Consequently, the thickness of the momentum boundary layer reduces with an increase in Mn. A similar trend may be observed in the case of β and Mn (see Fig. 4(a-b)).

The significance of λ_T and λ_C on profiles $f'(\eta)$, $\theta(\eta)$ and $\phi(\eta)$ is portrayed in Figs.5 (a-c). For larger values of λ_T there is a rise in $f'(\eta)$. Physically, the positive values of λ_T corresponds to assisting flow and negative values of λ_T results opposing flow, whereas $\lambda_T = 0$ shows the absence of buoyancy forces. However, quite opposite pattern may be observed in the case of $\theta(\eta)$ and $\phi(\eta)$. A similar behavior may be observed in the case of concentration buoyancy parameter λ_C. Fig.6 is drawn for different values of velocity slip parameter α_2 and Magnetic parameter Mn on velocity profile. For increasing values of α_2 initially the velocity profiles decreases and gradually increases as away from the sheet. The impact of Eckert number Ec and heat source/sink parameter λ on temperature profile is drawn in Fig.7. The temperature of the fluid enhances as Eckert number increases and the phenomenon is due to the relation between Ec and temperature difference, that is, $Ec \propto 1/(T_w - T_\infty)$, heat source/sink parameter λ also shows similar pattern. Fig.8 is drawn to explain the effects of distinct values of $\Pr$ and Bi_T on $\theta(\eta)$. It is evident from the figure that the temperature profile reduces for larger values of $\Pr$. Clearly, higher values of Pr indicate a large heat capacity, which intensifies the heat transfer. Therefore, the cooling of the heated sheet can be improved by choosing a coolant with a large Pr. The temperature of the fluid increases as Biot number Bi_T extends, since Bi_T is directly proportional to the heat transfer coefficient h_T, due to this Bi_T cause's stronger convection which leads to increment in the temperature profile. The influence of Brownian motion parameter Nb and thermophoresis parameter Nt on $\theta(\eta)$ and $\phi(\eta)$ are presented in Figs. 9(a-b). It is inspected that for higher values of Nb temperature profiles enhances and concentration distribution reduces. In the case of Nt both temperature and concentration distribution enhances, this is due to the mechanism of thermophoresis which defined as nanoparticles move from hotter region to colder region; as a result temperature distribution rises. Fig.10 is plotted for different values of Lewis number Le and chemical reaction Kc on the concentration distribution. For higher values of Le concentration distribution reduces. Since Le has inverse relation with Brownian diffusion coefficient D_B, this leads to a decrease in the

thickness of the nanoparticle concentration boundary layer. Similar effect is observed in the case of chemical reaction Kc. Physically, $Kc > 0$ gives a destructive chemical reaction and for $Kc < 0$ yields constructive chemical reaction, whereas $Kc = 0$ shows the absence of chemical reaction. Fig.11 is drawn for different values of Lewis number Le and solutal Biot number Bi_C. Concentration profiles increases for larger values of Bi_C, this is to the fact that solutal Biot number is directly proportional to the heat transfer coefficient h_C

Effect of physical parameters on $-f''(0), -\theta'(0)$ and $-f'(0)$: The effect of different physical parameters on the skin friction coefficient $-f''(0)$, Nusselt number $\theta'(0)$ and Sherwood number $\phi'(0)$ are numerically presented in Table 4. The skin friction coefficient reduces for higher values of $Mn, \beta_1, A1$ and enhance for Q, λ_T, λ_C. It doesn't alter for remaining parameters. The Nusselt number extends for higher values of $Mn, \beta_1, \lambda, Ec, Nb, Nt, Bi_T$ and reduces for $m, A1, Q, \lambda_T, \lambda_C$ Pr. Remaining parameters does not alter. In the same manner the Sherwood number falls for greater values of $Q, \lambda_T, \lambda_C, A1, Nb, Le, Kc$ and enhances for Nt, Bi_C. Concentration distribution does not affect for other parameters. The present results are compared with the previous result which is shown below in Table.3.

Table 3: Comparison of results for $f''(0)$ when $\lambda_T = \lambda_C = Nb = Nt = Ec = Kc = Le = Bi_T = Bi_C = \alpha_2 = 0$ and $\alpha = \beta = 0.2, Mn = 0.1, Pr = 1$

Mn	Akbar et al.[9]	Malik et al.[10]	Imad Khan et al.[12]	Present result
0	-1	-1	-1	-1
0.5	-1.11803	-1.11802	-1.11802	-1.11800
1.0	-1.41421	-1.41429	-1.41423	-1.41422
5.0	-2.44949	-2.44945	-2.44945	-2.44821

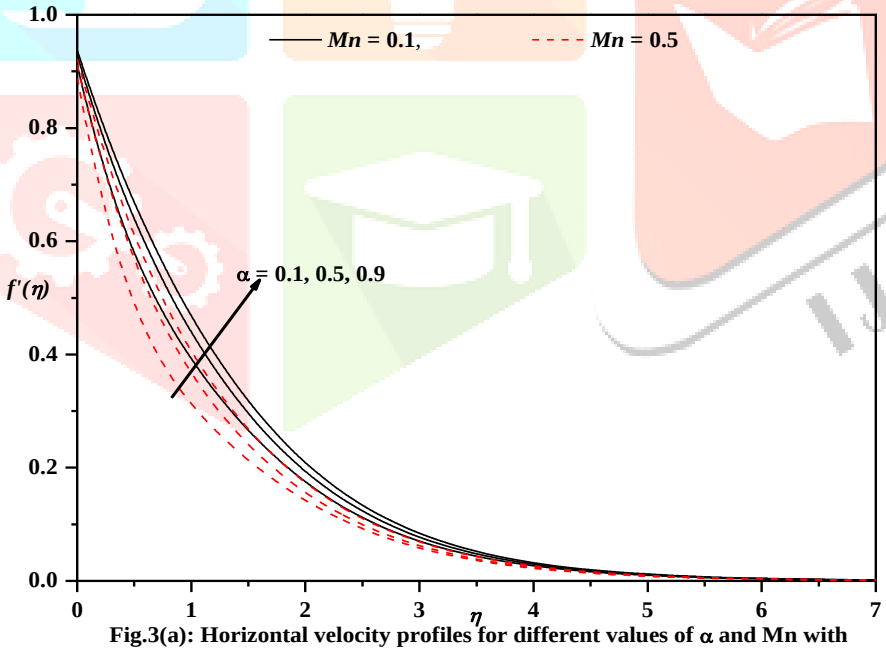

Fig.3(a): Horizontal velocity profiles for different values of α and Mn with $\alpha_2 = \lambda = Ec = Kc = 0.1$, $Nb = Nt = 0.2$, $\beta = \lambda_T = \lambda_C = 0.3$, $Le = 0.22$, $Pr = Bi_T = Bi_C = 1$.

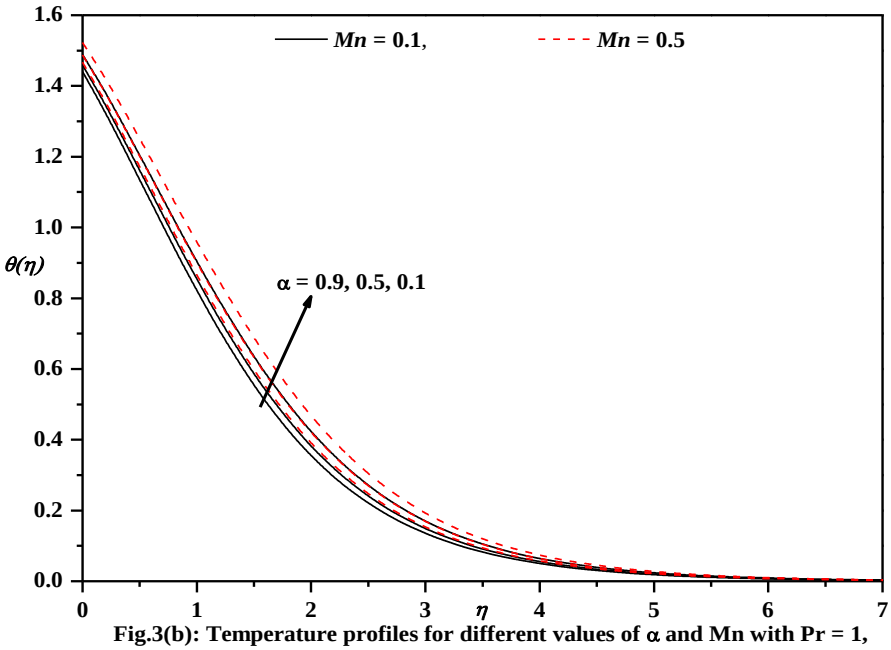

Fig.3(b): Temperature profiles for different values of α and Mn with Pr = 1, α_2 = λ = Ec = Kc = 0.1, Nb = Nt = 0.2, β = $\lambda_T = \lambda_C$ = 0.3, Le = 0.22, Pr = Bi_T = Bi_C = 1.

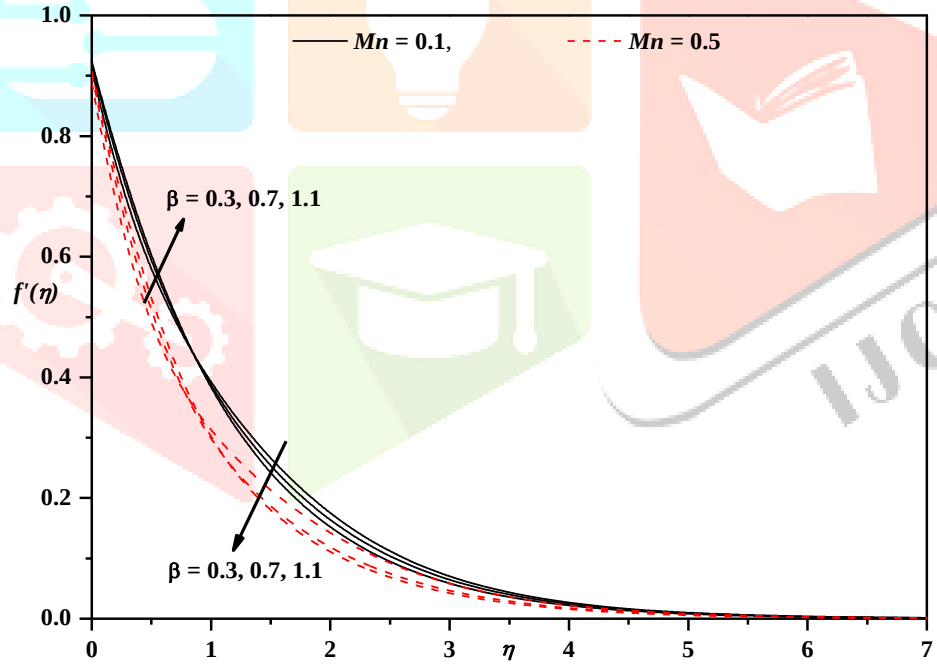

Fig.4(a): Horizontal velocity profiles for different values of β and Mn with Nb = Nt = 0.2, Kc = Ec = α = λ = α_2 = 0.1, $\lambda_T = \lambda_C$ = 0.3, Le = 0.22, Pr = Bi_T = Bi_C = 1.

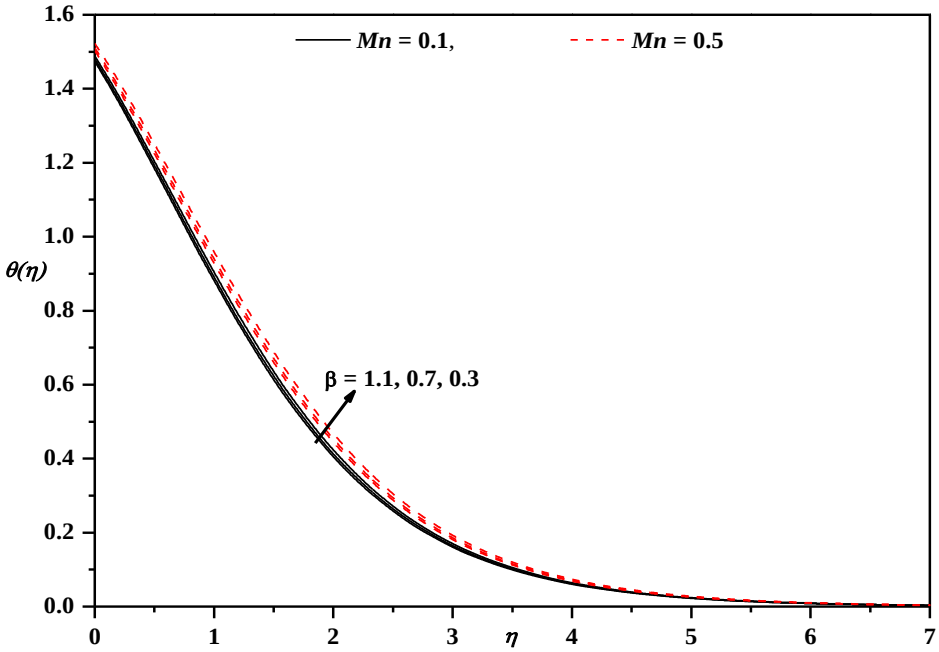

Fig.4(b): Temperature profiles for different values of β and Mn with Pr = 1, Nb = Nt = 0.2, Kc = Ec = α = λ = α_2 = 0.1, λ_T = λ_C = 0.3, Le = 0.22, Pr = Bi_T = Bi_C = 1.

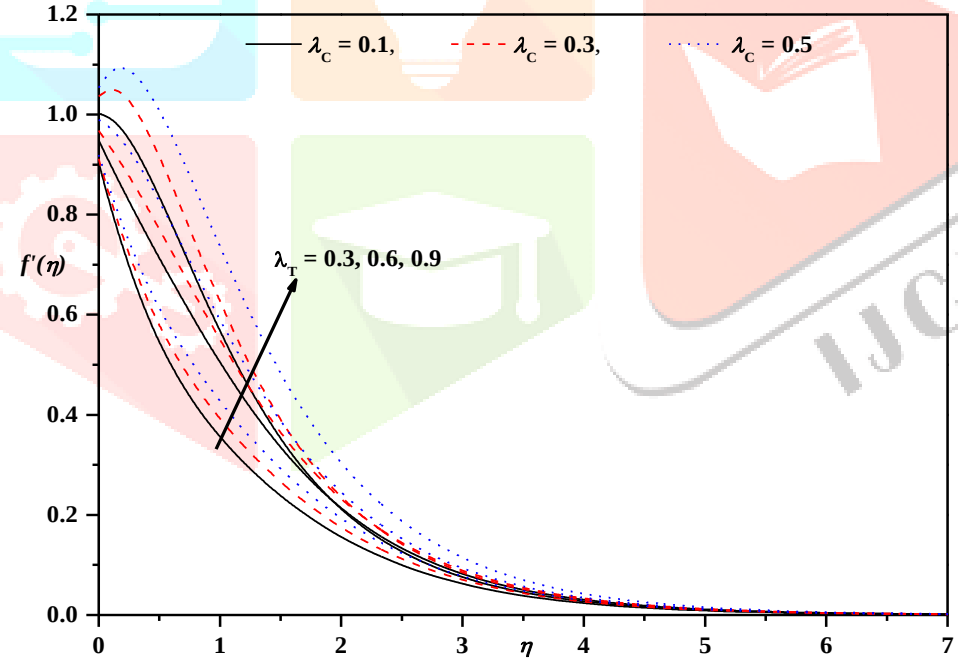

Fig.5(a): Horizontal velocity profiles for different values of λ_T and λ_C with Ec = Kc = Mn = α = α_2 = λ = 0.1, Nb = Nt = 0.2, β = 0.3,Le = 0.22, Pr = Bi_T = Bi_C = 1.

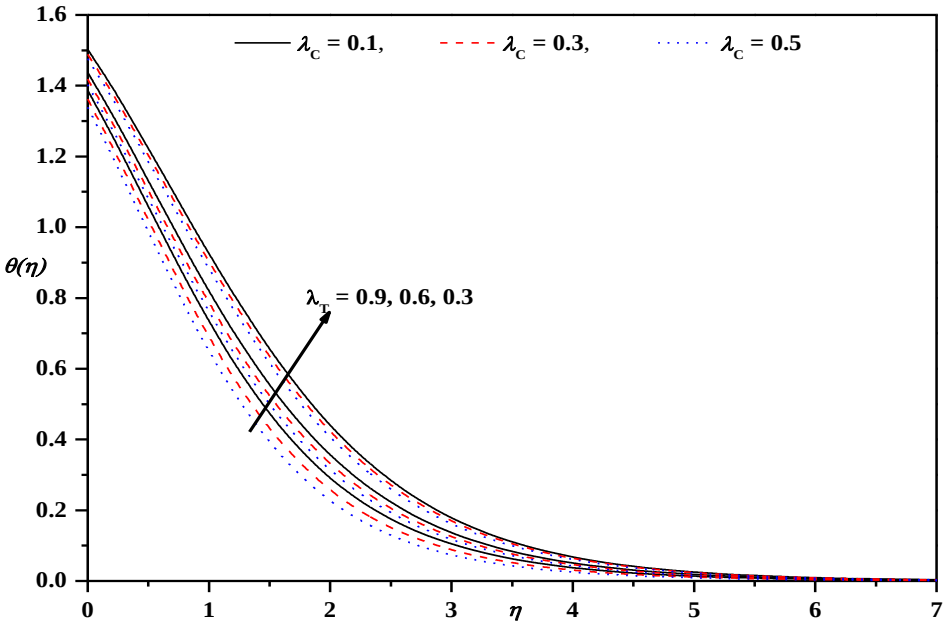

Fig.5(b): Temperature profiles for different values of λ_T and λ_C with Ec = Kc = Mn = α = α_2 = λ = 0.1, Nb = Nt = 0.2, β = 0.3, Le = 0.22, Pr = Bi_T = Bi_C = 1.

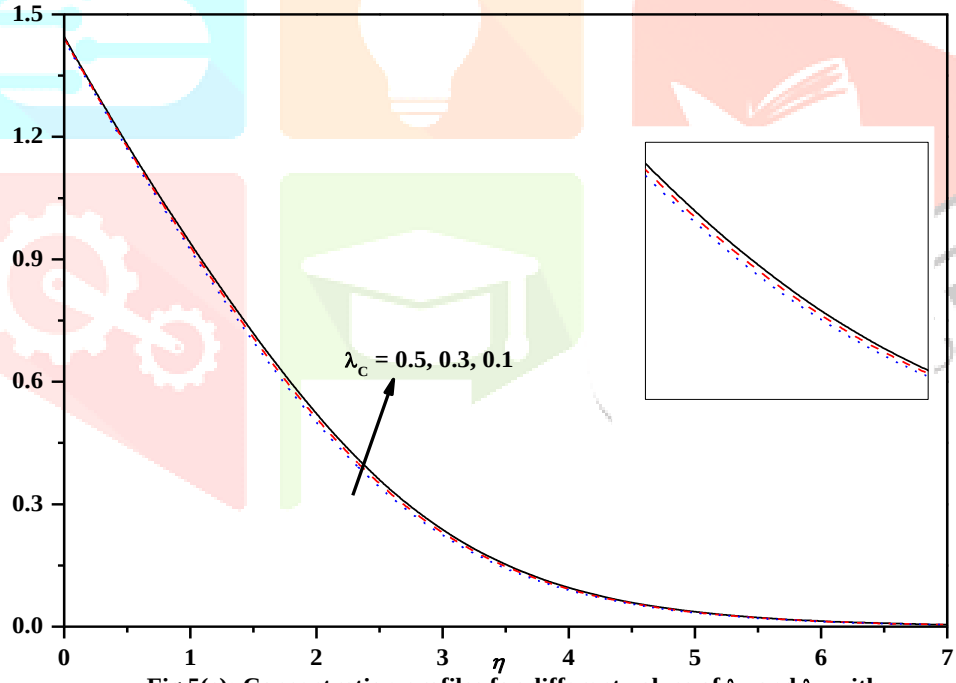

Fig.5(c): Concentration profiles for different values of λ_T and λ_C with Ec = Kc = Mn = α = α_2 = λ = 0.1, Nb = Nt = 0.2, β = 0.3, Le = 0.22, Pr = Bi_T = Bi_C = 1.

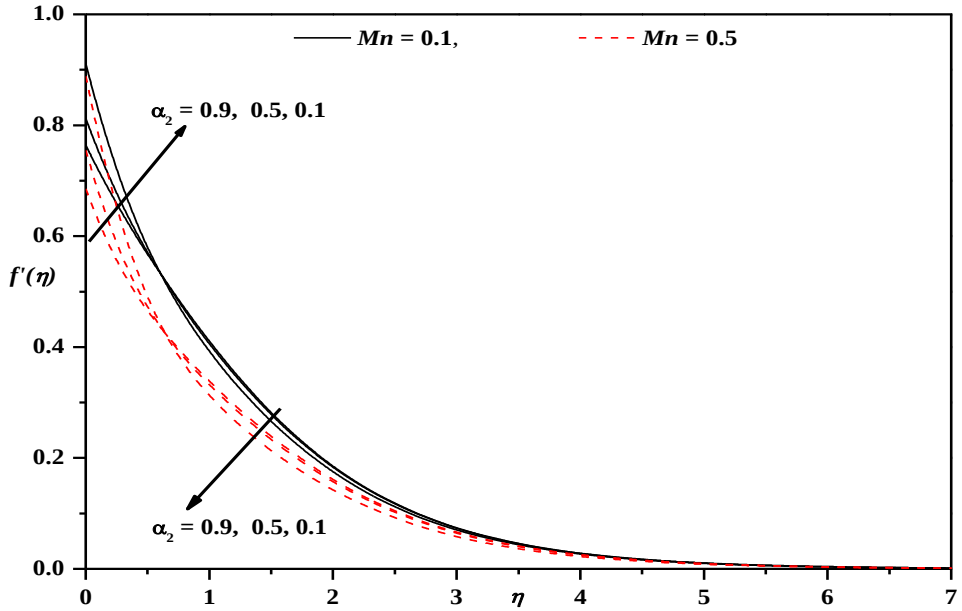

Fig.6: Horizontal velocity profiles for different values of α_2 and Mn with $\alpha = \lambda =$ Ec = Kc = 0.1, Nb = Nt = 0.2, $\beta = \lambda_T = \lambda_C = 0.3$, Le = 0.22, Pr = Bi_T = Bi_C = 1.

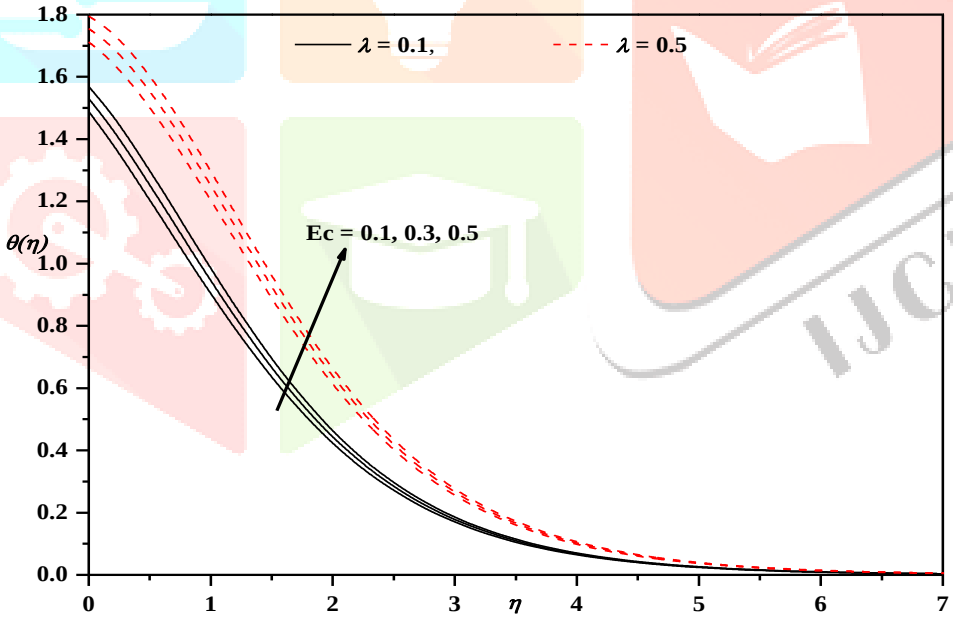

Fig.7: Temperature profiles for different values of Ec and λ with Nb = Nt = 0.2, Kc = Mn = $\alpha = \alpha_2 = 0.1$, $\beta = 0.3$, $\lambda_T = \lambda_C = 0.3$, Le = 0.22, Pr = Bi_T = Bi_C = 1.

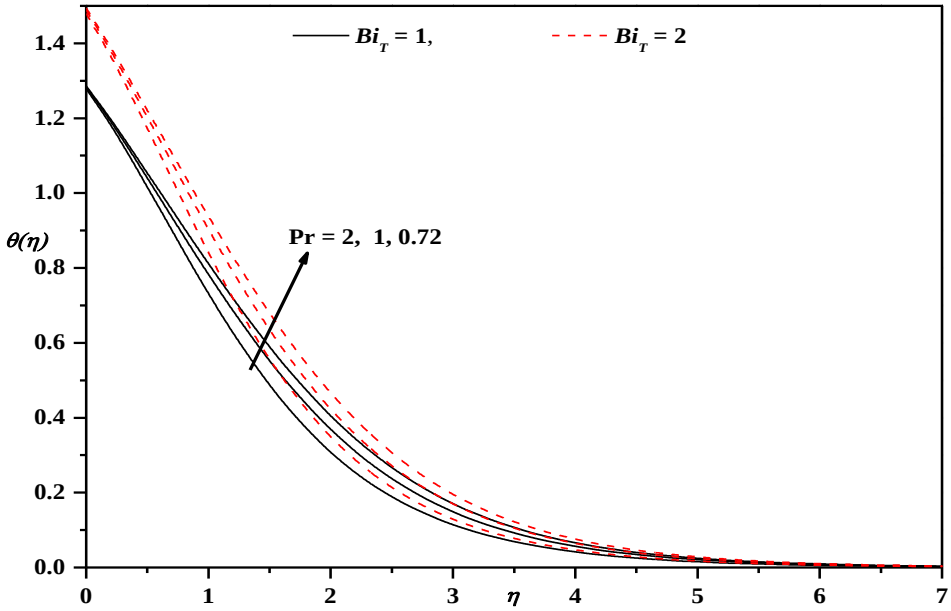

Fig.8: Temperature profiles for different values of Pr and Bi_C with Le = 0.22, Nb = Nt = 0.2, Mn = Kc = α = α_2 = λ = 0.1, β = 0.3, λ_T = λ_C = 0.3, Bi_C = 1.

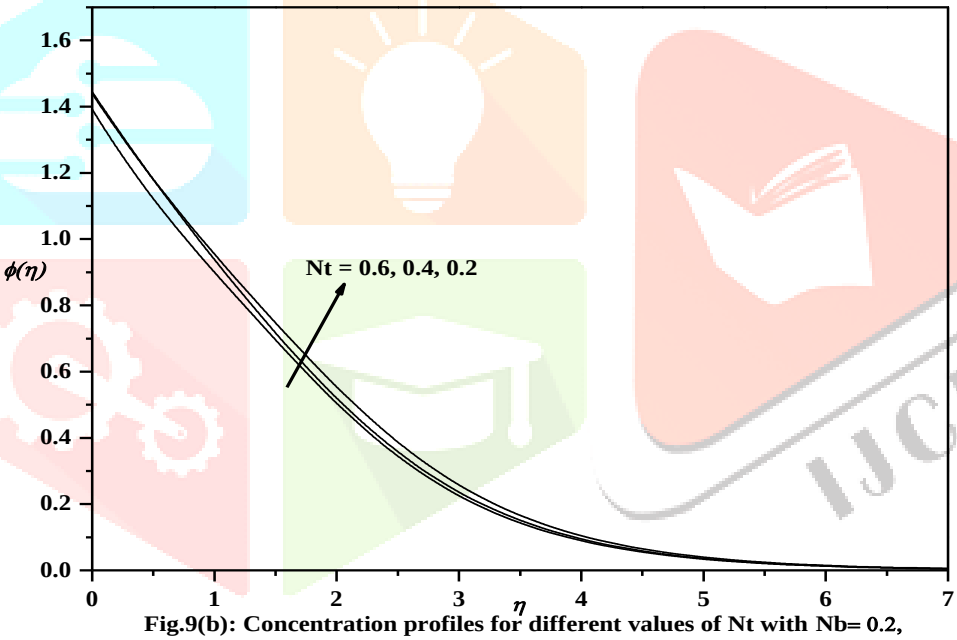

Fig.9(b): Concentration profiles for different values of Nt with Nb= 0.2, Kc = Mn = α = α_2 = λ = 0.1, β = 0.3, λ_T = λ_C = 0.3, Le = 0.22, Pr = Bi_T = Bi_C = 1.

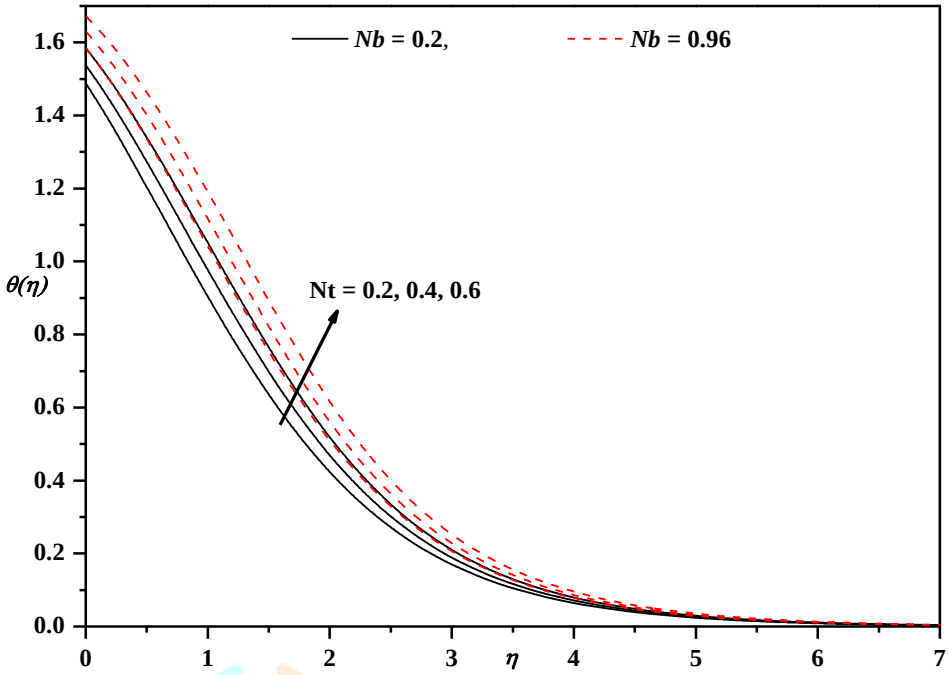

Fig.9(a): Temoerature profiles for different values of Nb and Nt with Kc = Mn = $\alpha = \alpha_2 = \lambda = 0.1$, $\beta = 0.3$, $\lambda_T = \lambda_C = 0.3$, Le = 0.22, Pr = $Bi_T = Bi_C = 1$.

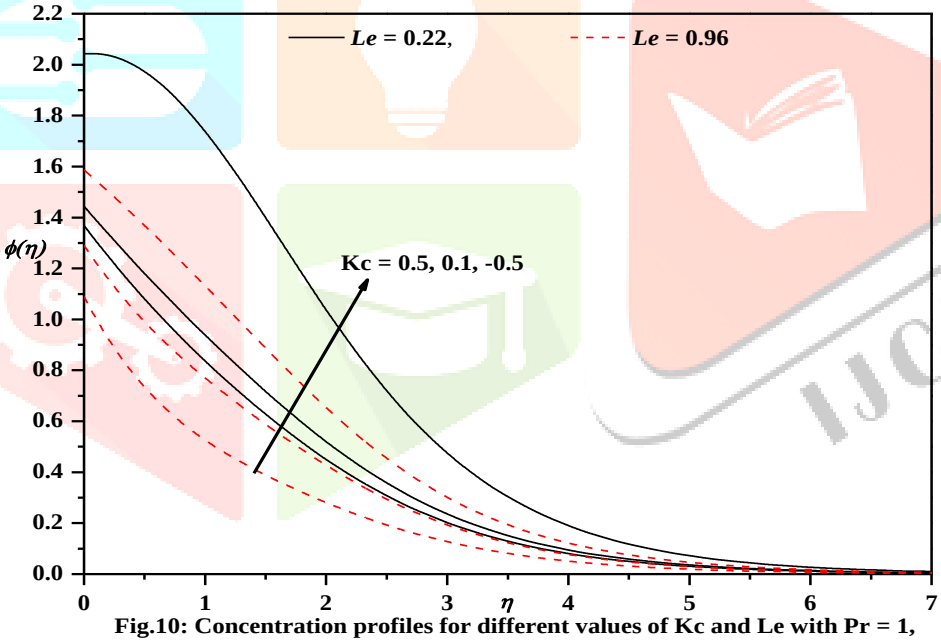

Fig.10: Concentration profiles for different values of Kc and Le with Pr = 1, Nb = Nt = 0.2, Mn = 0.1, $\alpha = 0.1$, $\beta = 0.3$, $\lambda = 0.1$, $\lambda_T = \lambda_C = 0.3$, $\alpha_2 = 0.1$, $Bi_T = Bi_C = 1$.

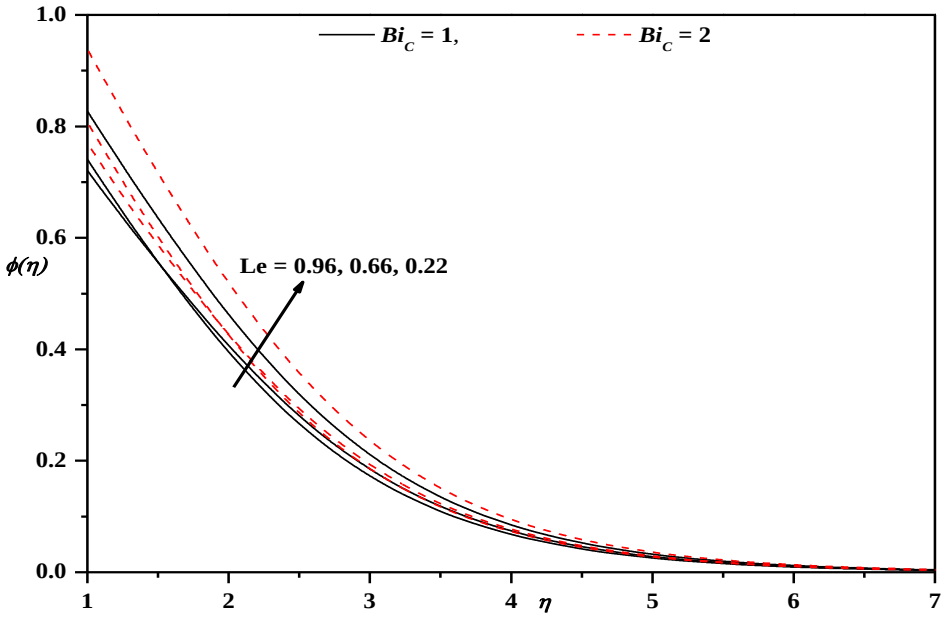

Fig.11:Concentration profiles for different values of Pr and Bi_C with Pr = 1, Nb = Nt = 0.2, Mn = Kc = $\alpha = \alpha_2 = \lambda = 0.1$, $\beta = 0.3$, $\lambda_T = \lambda_C = 0.3$, $Bi_T = 1$.

V. CONCLUDING REMARKS OF THE PRESENT WORK: In this work we studied the effect of mixed convective Prandtl nanofluid flow over a viscous stretching sheet in the presence of thermal and solutal Biot numbers. The physical behavior of the governing parameters is exhibited through graphs and the important key points of the present work as given below:

- The velocity profiles enhance and temperature profiles declines for increasing values of Prandtl parameters α and β.
- For higher values of thermal buoyancy parameter the velocity profiles extends and quite opposite results can be observed in the case of temperature and concentration profiles.
- For larger values of α_2 initially the velocity profiles decreases and gradually increases as away from the sheet.
- The temperature of the profiles enhances for increasing values of Eckert numb
- The temperature profile accelerates for higher values of thermal Biot number. A similar pattern can found in the case of solutal Biot number.
- For extending values of Nb temperature profiles enhances and concentration profiles reduces. But in the case of Nt, both temperature and concentration profiles enhances.
- For higher values of Le concentration distribution reduces.

REFERENCES

[1] Sakiadis, B.C. 1961. Boundary layer behavior on continuous solid surfaces. American Institute of Chemical Engineers Journal, **7**: 26–28.

[2] Crane, L.J. 1970. Flow past a stretching plate. Zeitschrift für angewandte Mathematik und Physi*k*. **21:** 645–647.

[3] Chen C.K. and Chen M.I. 1988. Heat transfer of a continuous stretching surface with suction or blowing. J. Math. Anal. Appl., 135: 568-580.

[4] Cortell, R. 2005. Flow and heat transfer of a fluid through a porous medium over a stretching surface with internal heat generation/absorption and suction/blowing. Fluid Dynamics Research, 37: 231-245.

[5] Abel M.S. and Mahesh N. 2008. Heat transfer in MHD viscoelastic fluid over a stretching sheet with variable thermal conductivity, Appl Math Modell, 32 (2008), 1965-83.

[6] Ishak, A., Nazar, R. and Pop, I. 2009. Boundary layer flow and heat transfer over an unsteady stretching vertical surface. Mecahnica, 44: 369-375.

[7] Prasad, K.V., Santhi S.R. and Datti, P.S. 2012. Non-Newtonian power law fluid flow and heat transfer over a non-linearly stretching sheet. Applied Nano Science, 3: 425-35.

[8] Akbar, N.S., Nadeem, S., Haq, R.U., and Khan, Z.H. 2013. Numerical solutions on magnetohydrodynamic boundary layer flow of tangent hyperbolic fluid towards a stretching sheet. Indian Journal of Physics, 87: 1121-1124.

[9] Akbar, N.S., Ebaid,A. and Khan. Z.H. 2015. Numerical analysis of magnetic field effects on Eyring-Powell fluid flow towards a stretching sheet. Journal of Magnetism and Magnetic Materials, 382: 355-358.

[10] Malik, M.Y., Salahuddin, T., Arif Hussain and Bilal, S. 2015. MHD flow of tangent hyperbolic fluid over a stretching cylinder: using Keller box method. Journal of Magnetism and Magnetic Materials, 395: 271-276.

[11] Rashidi, M.M., Bagheri, S., Mominiat, E. and Freidoonimehr 2017. Entropy analysis of convective MHD flow of third grade non-Newtonian fluid over a stretching sheet. Ain Shams Engineering Journal, 8: 77-85.

[12] Khan, I., Hussain. A. and Malik, M.Y. 2019. On magneto hydrodynamics Prandtl fluid flow in the presence of stratification and heat generation. physics A: Statistical mechanics and its applications, Vol. 540: https://doi.org/10.1016/j.physa.2019.123008.

[13] Choi, S.U.S. 1995. Enhancing thermal conductivity of fluids with nanoparticles. Developments and Applications of Non-Newtonian Flows, 66: 99-105.

[14] Buongiorno, J. 2006. Convective transport in nanofluids. ASME J. Heat Transfer, 128(3): 240-250.

[15] Rana, P., and Bhargava, R. 2012. Flow and heat transfer of a nanofluid over a nonlinearly stretching sheet, Commun Nonlinear Sci Numer Simul, 17: 212-216.

[16] Prasad, K.V., Hanumesh Vaidya, Vajravelu, K. and Ramanjini, V. 2018. Analytical study of Catteno – Christov heat flux model for Williamson Nanofluid flow over a slender elastic sheet with variable thickness. Journal of Nanofluid, 7.3, 583-594.

[17] Uddin, M.J., Khan, W.A., and Md. Ismail A.I. 2018. Melting and second order slip effect on convective flow of nanofluid past aradiating stretching/shrinking sheet. Propulsion and Power Research, 7: 60–71.

[18] Hayat, T., ullah, S., Khan, M.I., Alsaedi, A. and Zia Q.A.Z. 2018. Non Darcy flow of water based carbon nanotubes with nonlinear radiation and heat generation/absorption. Results in physics, 8, 473-480.

[19] Prasad, K.V., Hanumesh Vaidya, Vajravelu, K. and Srikantha Setty, B. 2020. MHD Flow of a UCM Nanofluid in a Permeable Channel: Boungiorno's model. International Journal of Applied and Computational Mathematics, Springer, 6: 126 .

[20] Moutsoglou, A. and Chen, T.S. 1980. Buoyancy effects in boundary layers on inclined continuous moving sheets, J. Heat Trans.,102(2): 371-373.

[21] Vajravelu, K. 1994. Convection heat transfer at a stretching sheet with suction or blowing. J.Math.Analy.Appl., 188(3) 1002-1011.

[22] Das, S., Jana, R.N. and Makinde, O.D. 2015. Magneto hydrodynamic mixed convective slip flow over an inclined porous plate with viscous dissipation and joule heating, Alex. Eng. J., 54: 251-261.

[23] Prasad, K.V., Hanumesh Vaidya, Makinde, O.D. and Srikantha Setty, B. 2019. MHD mixed convective flow of Casson nanofluid over a slender rotating disk with source/sink and partial slip effects. Defect and Diffusion Forum, 392, 92-122.

[24] Liao, S. 2010. An optimal Homotopy – analysis approach for strongly nonlinear equations. Commu. Non-Linear. Sci. Num. Simu., 15: 2003- 2016.

[25] Fan T. and You. X. 2013. Optimal homotopy analysis method for nonlinear differential equations in the boundary layer. Numer. Algor., 62(2): 337-354.

[26] Van Gorder, R.A. 2019. Optimal homotopy analysis and control of error for implicitly defined fully nonlinear differential equations, Numer. Algor., 81: 181-196.

Table 4.Values of Skin friction, Nusselt number and Sherwood number with the computed CPU time (in seconds) for different physical parameters and fixed values of Le = 0.22, Ec =0.1, $Bi_T = Bi_C = 1$, $\lambda = \alpha_2 = 0.1$, at 10^{th} approximation.

Pr	*Kc*	*Nt*	*Nb*	λ_C	λ_T	*Mn*	β	α	$-f''(0)$	$-h_f$	E_{10}^f	$-\theta'(0)$	$-h_\theta$	E_{10}^θ	$\phi'(0)$	$-h_\phi$	E_{10}^ϕ	CPU time
1	0.22	0.2	0.2	0.3	0.3	0.1	0.3	0.1	0.8862	1.9913	8.80×10^{-5}	0.5101	1.5916	5.74×10^{-5}	0.5553	1.5205	2.52×10^{-4}	159.65
								0.5	0.7062	1.9065	3.32×10^{-6}	0.5407	1.5775	3.28×10^{-5}	0.5564	1.5520	2.64×10^{-4}	147.96
								0.9	0.6265	1.2535	2.55×10^{-5}	0.5593	1.4950	2.75×10^{-5}	0.5583	1.5000	2.83×10^{-4}	156.10
1	0.22	0.2	0.2	0.3	0.3	0.1	0.3	0.1	0.8862	1.9913	8.80×10^{-5}	0.5101	1.5916	5.74×10^{-5}	0.5553	1.5205	2.52×10^{-4}	159.65
							0.7		0.8033	1.8509	6.16×10^{-5}	0.5190	1.5928	6.22×10^{-5}	0.5555	1.5215	2.58×10^{-3}	144.09
							1.1		0.7616	1.5582	9.20×10^{-5}	0.5250	1.5912	6.31×10^{-5}	0.5556	1.5219	2.58×10^{-3}	178.72
1	0.22	0.2	0.2	0.3	0.3	0.1	0.3	0.1	0.8862	1.9913	8.80×10^{-5}	0.5101	1.5916	5.74×10^{-5}	0.5553	1.5205	2.52×10^{-4}	159.65
						0.5			1.1153	1.8356	1.41×10^{-5}	0.4768	1.6114	1.45×10^{-3}	0.5542	1.5199	2.38×10^{-3}	181.29
						0.9			1.3027	0.9350	4.41×10^{-4}	0.4508	1.6133	2.39×10^{-3}	0.5536	1.5181	2.29×10^{-3}	136.20
1	0.22	0.2	0.2	0.3	0.3	0.1	0.3	0.1	0.8862	1.9913	8.80×10^{-5}	0.5101	1.5916	5.74×10^{-5}	0.5553	1.5205	2.52×10^{-4}	159.65
					0.6				0.5159	1.9777	2.91×10^{-5}	0.5625	1.4988	6.21×10^{-6}	0.5576	1.5226	2.83×10^{-4}	177.85
					0.9				-0.0223	2.0819	5.71×10^{-4}	0.6128	1.5543	3.53×10^{-5}	0.5609	1.5258	3.22×10^{-4}	168.45
1	0.22	0.2	0.2	0.1	0.3	0.1	0.3	0.1	0.9630	2.0572	8.43×10^{-5}	0.4978	1.6035	9.95×10^{-5}	0.5548	1.5200	2.46×10^{-6}	139.40
				0.3					0.8862	1.9913	8.80×10^{-5}	0.5101	1.5916	5.74×10^{-5}	0.5553	1.5205	2.52×10^{-4}	159.65
				0.5					0.8059	1.9602	7.24×10^{-5}	0.5237	1.5764	2.91×10^{-5}	0.5558	1.5208	2.58×10^{-4}	164.20
1	0.22	0.2	0.2	0.3	0.3	0.1	0.3	0.1	0.8862	1.9913	8.80×10^{-5}	0.5101	1.5916	5.74×10^{-5}	0.5553	1.5205	2.52×10^{-4}	159.65
			0.4						0.8429	2.0623	5.86×10^{-5}	0.4148	1.5642	13.2×10^{-4}	0.5664	1.5460	2.34×10^{-4}	138.24
			0.6						0.8651	2.0362	8.69×10^{-5}	0.4620	1.5765	8.71×10^{-4}	0.5664	1.5460	2.34×10^{-4}	129.22
1	0.22	0.5	0.2	0.3	0.3	0.1	0.3	0.1	0.8862	1.9913	8.80×10^{-5}	0.5101	1.5916	5.74×10^{-5}	0.5553	1.5205	2.52×10^{-4}	159.65
		1.0							0.8621	1.9169	1.07×10^{-4}	0.4613	1.5690	9.82×10^{-5}	0.5609	1.4462	2.48×10^{-4}	158.86
		2.0							0.8403	1.9413	1.24×10^{-4}	0.4145	1.5552	1.75×10^{-4}	0.6079	1.3546	2.08×10^{-4}	177.31
1	-0.2	0.2	0.2	0.3	0.3	0.1	0.3	0.1	0.8674	2.0628	8.86×10^{-5}	0.5154	1.5844	4.49×10^{-5}	0.4133	1.5573	1.04×10^{-4}	123.04
	0.5								0.8862	1.9913	8.80×10^{-5}	0.5101	1.5916	5.74×10^{-5}	0.5553	1.5205	2.52×10^{-4}	159.65
	1.0								0.8961	1.9803	7.97×10^{-5}	0.5086	1.5951	6.46×10^{-5}	0.6312	1.4924	8.87×10^{-5}	124.09
0.72	0.22	0.5	0.5	0.1	0.2	0.1	0.2	0.2	0.8781	1.9803	1.24×10^{-4}	0.5051	1.6274	1.62×10^{-4}	0.5530	1.5321	2.18×10^{-5}	146.78
1.0									0.8862	1.9913	8.80×10^{-5}	0.5101	1.5916	5.74×10^{-5}	0.5553	1.5205	2.52×10^{-4}	159.65
2.0									0.9007	1.9552	4.22×10^{-4}	0.5204	1.4112	4.36×10^{-6}	0.5590	1.5040	3.25×10^{-5}	159.88